

(N-Heterocyclic Carbene)-Palladate Complexes in Anionic Mizoroki–Heck Coupling Cycles: A Combined Experimental and Computational Study

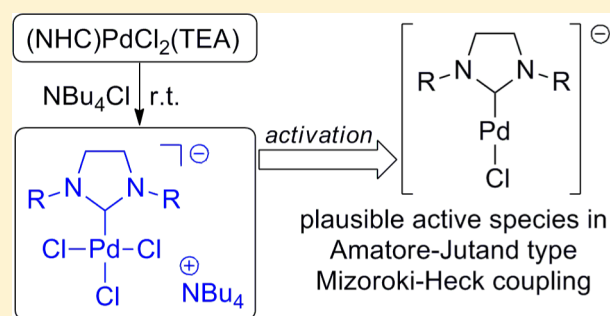
Daniel Guest,[†] Vitor H. Menezes da Silva,[‡] Ana P. de Lima Batista,[‡] S. Mark Roe,[†] Ataulpa A. C. Braga,^{*,‡} and Oscar Navarro^{*,†}

[†]Department of Chemistry, University of Sussex, Brighton, BN1 9QJ, United Kingdom

[‡]Departamento de Química Fundamental, Instituto de Química, Universidade de São Paulo, São Paulo, São Paulo, 05508-000, Brazil

Supporting Information

ABSTRACT: The reaction of complex (SIPr)PdCl₂(TEA) (SIPr = 1,3-bis(2,6-diisopropylphenyl)-2-imidazolidinylidene, TEA = triethylamine) with tertbutylammonium chloride (TBAC) at room temperature affords the new ionic complex [TBA][(SIPr)PdCl₃] in quantitative yield. The activity of this complex as a precatalyst for Heck coupling reactions has been explored. Experimental results and DFT calculations support a plausible anionic Amatore–Jutand-type mechanism for the Heck reaction involving anionic (NHC)-palladium(0) catalytic species.

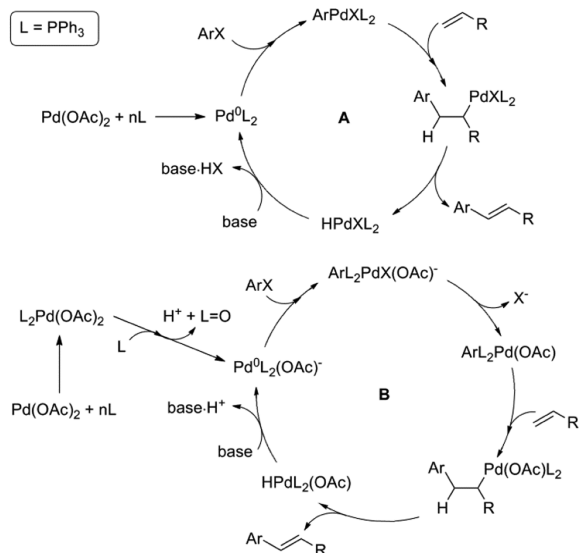


INTRODUCTION

The Mizoroki–Heck reaction, involving the coupling of organic halides or pseudohalides with alkenes, is one of the most studied and utilized palladium-catalyzed reactions.¹ The “textbook” catalytic cycle is depicted in Scheme 1 (A), involving the oxidative addition of the halide, *syn* addition and β -hydride elimination of the alkene, followed by reductive

elimination of the coupling product. Unfortunately, the mechanism of the reaction is far more complicated than this and is greatly affected by the different components of the reaction: coupling partners, solvent, base, additives, temperature, and even the nature of the catalyst/precatalyst. This complexity has resulted in extensive and detailed studies, both experimental and theoretical, which have emphasized even more the particular character of this ubiquitous reaction.^{2,3}

Scheme 1. “Textbook” (A) and Amatore–Jutand (B) Heck Catalytic Cycles



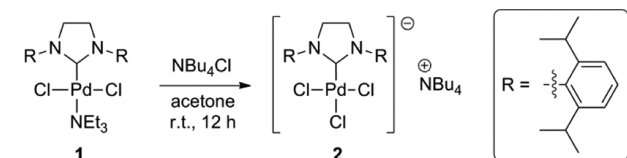
A very important contribution to the body of knowledge on this reaction was made by Amatore and Jutand in the 1990s, proposing a Heck mechanism that diverged from the classical one in that in-situ-formed anionic species played a key role in nonligandless, homogeneous systems:⁴ using electrochemical techniques they postulated that in Pd(OAc)₂ + phosphine mixtures the anionic 16-electron species (PPh₃)₂Pd(OAc)[−] undergoes oxidative addition with aryl halides, generating short-lived anionic pentacoordinated arylpalladium(II) complexes. This key modification resulted in the commonly known Amatore–Jutand Heck cycle (Scheme 1 (B)), which can be in fact extended to all palladium cross-coupling reactions. Moreover, the authors remark on the effect of ionic additives in the reaction such as TBAC (TBAC = tetrabutylammonium chloride) on the formation of active anionic species such as L₂Pd(0)Cl[−], stabilized by the corresponding cation.⁵ All this work was compiled in two excellent reviews published in 1999 and 2000.⁶

Special Issue: Mike Lappert Memorial Issue

Received: November 28, 2014

Our group recently reported on the use of (NHC)-PdCl₂(TEA) complexes (NHC = N-heterocyclic carbene, TEA = triethylamine)⁷ as precatalysts for Heck couplings of unactivated aryl bromides and activated aryl chlorides with alkenes,⁸ following standard Jeffery reaction conditions.⁹ In that protocol we made use of tetrabutylammonium bromide (TBAB) in equimolar quantities as additive, after realizing that reactions carried out in its absence did not afford the desired products. More recently, we have decided to further investigate the effect of the quaternary salt on the catalytic process. An initial screening of the same substrates subjected to the same reaction conditions but substituting TBAB with TBAC showed that the reaction outcome was not altered by this modification. We then turned our attention to the effect of the additive on the precatalyst, (SIPr)PdCl₂(TEA) (**1**) (SIPr = 1,3-bis(2,6-diisopropylphenyl)-2-imidazolidinylidene). The reaction of **1** with TBAC in anhydrous acetone, in air and at room temperature, led to the formation of the novel ionic complex [TBA][(SIPr)PdCl₃] (**2**) in 88% yield in 5 h, quantitatively if the reaction time was extended to 12 h

Scheme 2. Synthesis of [(SIPr)PdCl₃][TBA]



(Scheme 2). This complex was fully characterized by ¹H and ¹³C NMR and elemental analysis. Slow evaporation of a solution of **2** in technical grade acetone and hexane led to the formation of crystals suitable for X-ray diffraction, in which a molecule of water cocrystallized with a molecule of **2** (Figure 1). In the complex, the Pd center adopts an expected square planar geometry. Regarding the bond distances in the anion, the Pd1–Cl2 distance is longer than the other two Pd1–Cl bonds, due to the *trans* influence imparted by the NHC. The Pd–Cl distance is, as expected, in the range of a single bond and slightly shorter than that for **1** (1.959(2) vs 1.970(3) Å, respectively).¹⁰ The structure features a tetrabutylammonium cation, with a separation distance of 4.62 Å between the closest chlorine and the quaternized nitrogen.

A literature search revealed that while non-NHC-bearing complexes of the type [NR₄][LPdX₃] (L = amine, arsine, phosphine; X = halide) were already described in the early 1970s,¹¹ only one previous example of an [(NHC)PdX₃][−] anion has been reported, featuring a benzylimidazolium as cation (Figure 2, **3**).¹² A handful of other [(NHC)PdX₃][−] complexes have been reported in which the negative charge is neutralized by a pendant imidazolium or triazolium N-substituent in the NHC (Figure 2, **4–6**).¹³ To the best of our knowledge, the use of these complexes in catalysis has not been explored.

We then carried out test reactions to explore the possibility that **2** could be generated in situ in our previous protocol for the Heck reaction, playing the role of catalyst precursor in an Amatore–Jutand Heck-type mechanism. The reduction of (NHC)-Pd(II) complexes to the corresponding (NHC)-Pd(0) species by carbonate bases at high temperatures is well documented¹⁴ and in our case would potentially lead to the formation of an [(NHC)Pd(0)Cl][−] species that could start the

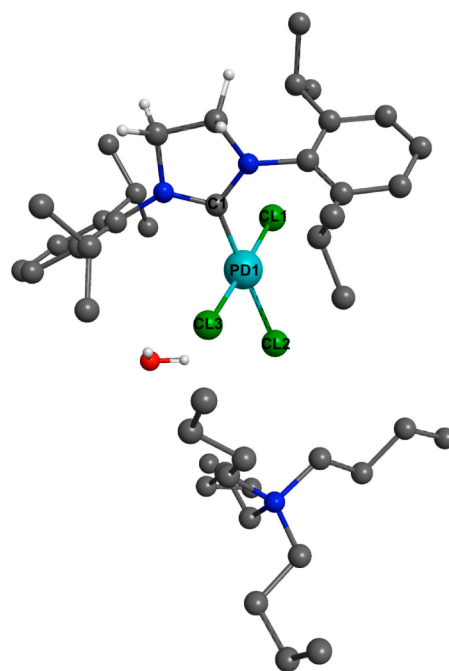


Figure 1. Crystal structure of [TBA][(SIPr)PdCl₃] (**2**), cocrystallized with one molecule of H₂O. Hydrogen atoms are omitted for clarity except those in the backbone of the NHC. Selected bonds (Å) and angles (deg): C1–Pd1: 1.959(2); Pd1–Cl2: 2.3770(7); Pd1–Cl1: 2.3020(6); Pd1–Cl3: 2.3080(6); C1–Pd1–Cl1: 89.89(6); C1–Pd1–Cl3: 88.61(6).

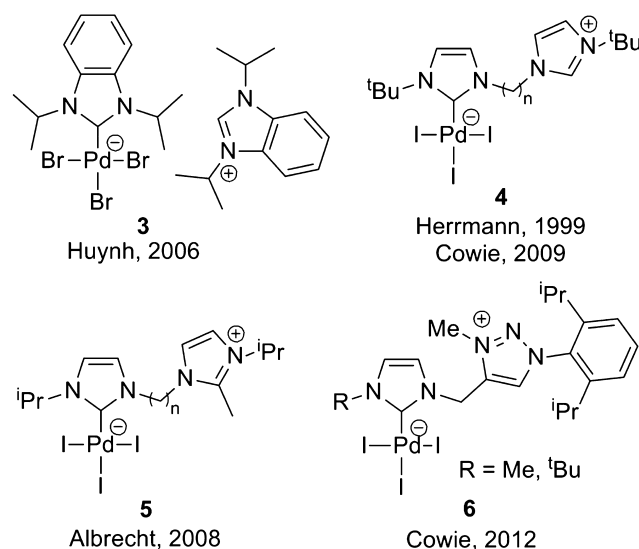
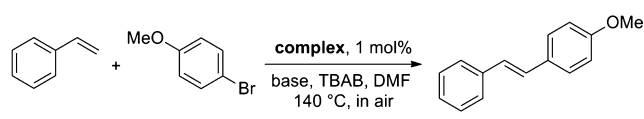


Figure 2. Previous examples of [(NHC)PdX₃][−]-containing complexes in the literature (X = halide).

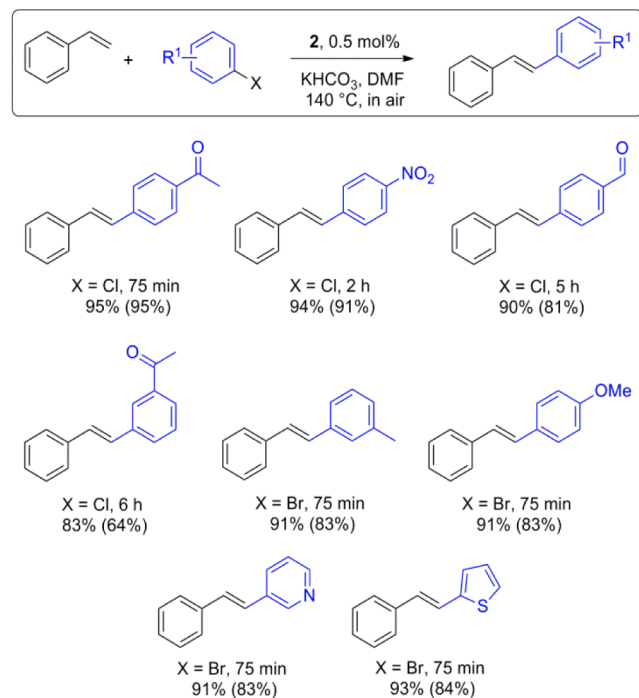
catalytic cycle. In a first comparison to the use of **1** + TBAC (Table 1, entry 2), we found that **2** performed as well for the coupling of 4-Br-anisole and styrene under the same reaction conditions (Table 1, entry 3) in the absence of the quaternary salt. The addition of 1 equiv (0.5 mmol) of TBAC to a reaction catalyzed by **2** did not increase the yields nor reduce the reaction time (Table 1, entry 4), reinforcing further that the role of the ammonium salt in our early protocol was solely to participate in the formation of **2**. Switching the base to HCO₃[−]¹⁵ led to a considerable decrease in the reaction time (Table 1, entry 5), which ultimately allowed us to decrease the

Table 1. Comparison of the Activity of **1** and **2** in the Coupling of 4-Br-Anisole and Styrene^a


entry	complex	base	yield (%)	time (min)
1 ^b	1	K ₂ CO ₃	92	60
2 ^c	1	K ₂ CO ₃	93	75
3 ^d	2	K ₂ CO ₃	91	75
4 ^c	2	K ₂ CO ₃	91	75
5 ^d	2	KHCO ₃	94	30
6 ^e	2	KHCO ₃	97	75

^aReaction conditions: 2-Br-anisole, 0.5 mmol; styrene, 0.55 mmol; TBAB, 0.5 mmol; base, 1 mmol; DMF, 1 mL; complex, 1 mol %. ^bSee ref 8. ^cTBAC instead of TBAB. ^dNo TBAB. ^eNo TBAB, complex loading 0.5 mol %.

catalyst loading by half without any detriment to the yield of the desired product (Table 1, entry 6). With these new optimized reaction conditions, a variety of aryl bromides and chlorides were coupled with styrene (Scheme 3). In all cases, the yields obtained are equal to or higher than those obtained using **1** + TBAB in comparable reactions times (in parentheses).

Scheme 3. Heck Couplings of Aryl Chlorides and Bromides with Styrene

To gain further insight into the mechanism under this specific set of conditions and the potential role of an [(NHC)PdCl][−] species (**7**), computational studies were carried out on a model system in which, for simplicity, the 2,6-diisopropyl groups were replaced by methyl groups. The use of model systems is a common tool in computational chemistry to provide insights into their respective real systems,^{16–20} often yielding very good results.

The coupling between PhBr (**8**) and styrene (**9**) in the presence of HCO₃[−] (**10**) as the base was considered. The explored mechanism is based on experimental evidence of anionic palladium complexes as the reactive species in the catalytic cycle.^{6b,21} Anionic Pd complexes are more likely to be found in a reaction medium using polar solvents and under high temperature,^{22,23} i.e., conditions similar to the one employed in the current experimental work. In addition, theoretical findings have proposed plausible catalytic cycles involving anionic palladium intermediates in analogous cross-coupling reactions.^{24,25} The overall computed profile of this model reaction is displayed in Figure 3. The prefixes **I** and **TS** stand for intermediates and transition states, respectively, in the text. As shown in the energy profile of Figure 3, there are four main steps in the considered Heck catalytic cycle: oxidative addition, migratory insertion, β-hydride elimination, and reductive elimination. Although the first and last steps are more sensitive to the nature of the solvent, the general energetic trends are maintained throughout the reaction path. The energetic difference between products and reactants is −50.3 kcal mol^{−1}, characterizing a quite exoergic process. The overall reaction profile goes downhill and occurs very smoothly. In the first step, bromobenzene adds to the [(NHC)PdCl][−] species. Scheme 4 presents the proposed mechanism for the oxidative addition step, and Figure 4 shows optimized geometries of selected structures (**II** and **TS1**) for this process. The initial approach between the catalyst **7** and the reactant **8** yields the intermediate **II**. It corresponds to the coordination of the benzene ring to the Pd complex through an η²-coordination mode. This intermediate is −10.4 kcal mol^{−1} with respect to the separated reactants. The oxidative addition process continues through **TS1** to yield the intermediate **I2**. The formation of **I2** is quite exoergic (−43.5 kcal mol^{−1}) and goes through **TS1**, which is higher by 4.7 kcal mol^{−1} in relation to **II**. Clearly, the oxidative addition is the rate-determining step of the overall reaction mechanism. The energy profile for this reaction shows the anionic oxidative addition step as a suitable and irreversible process. The inclusion of the effect of the solvent raises this value to 9.1 kcal mol^{−1} above the separated reactants. In the overall profile, it is noted that the solvent has the greatest influence over the oxidative addition step. This behavior was expected, because herein there is a bulky charged transition state that is largely affected by the action of the polar solvent. Once the oxidative addition has been accomplished, in order to continue the Heck reaction, the olefin **9** should replace the Br[−] ligand in the coordination sphere of the Pd center in the intermediate **I2**. Despite our efforts, we were unable to locate a transition state for the direct Br[−] substitution by **9**. Given the fact that a vacant coordination site is necessary to allow the olefin coordination to the metal center and that Pd–Cl and Pd–NHC bonds are stronger than the Pd–Br bond,²⁶ the Pd–Br bond dissociation was assumed. Several constrained optimizations along a LLM (linear least motion) path were performed in order to estimate the value of an existing dissociation barrier of the Pd–Br bond. It was possible to infer that the bromine dissociation should either involve a very small barrier or not proceed through a saddle point on the explored potential energy surface (PES). The LLM was obtained by using MacMolPlt.²⁷ After Br[−] leaves the metal center, the system becomes neutral.

The insertion of **9** into the vacant site can create two possible intermediates, **I3a** and **I3b** (Figure 5). The structure of **I3b** shows that the olefin is coordinated following a perpendicular

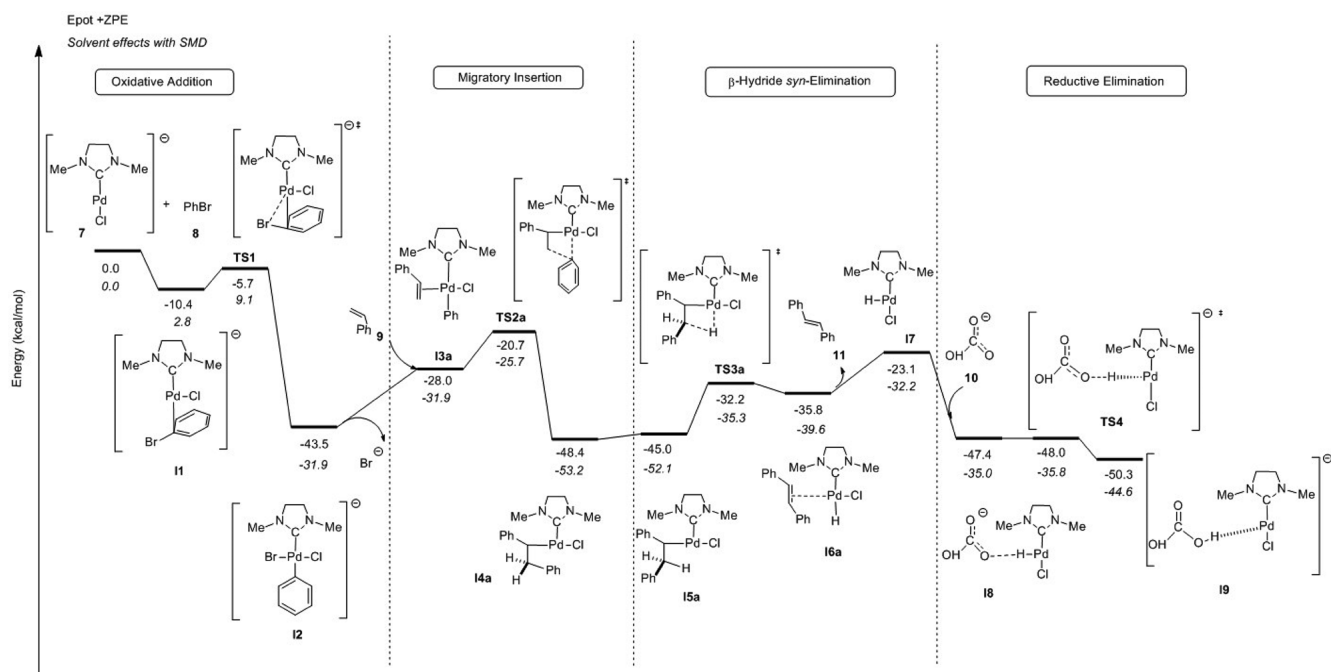


Figure 3. M06L/6-31+G(d) integrated relative energy profile for a plausible pathway on the studied model Mizoroki–Heck system reaction. M06L-SMD/6-31+G(d)//M06L/6-31+G(d) energies are in italics. All energies are given in kcal mol⁻¹ with respect to the infinitely separated reactants. Only the stationary points with the lowest energy in the explored PES (potential energy surface) are shown.

Scheme 4. Proposed Mechanism for the Oxidative Addition

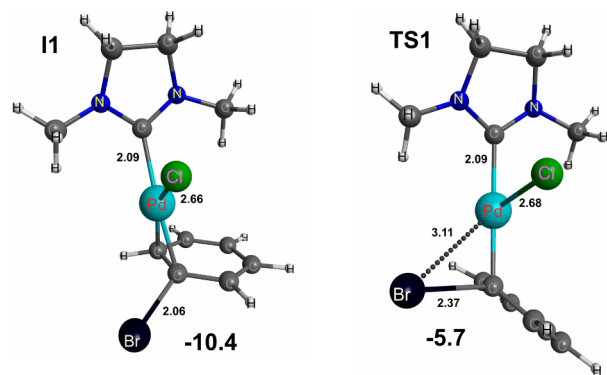
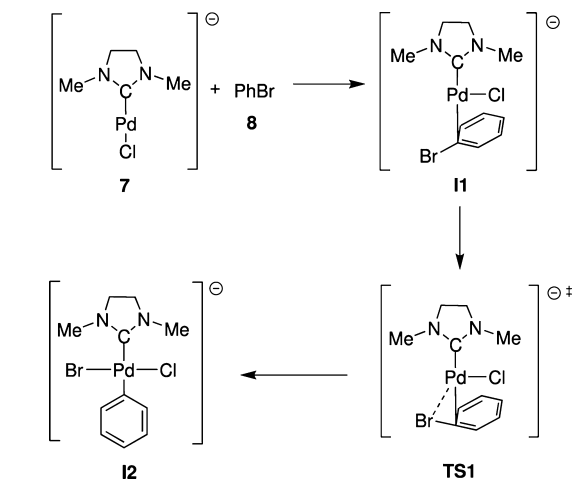


Figure 4. Optimized structures of intermediate **11** and the transition state **TS1** for the anionic oxidative addition step. Relative energies are given in kcal mol⁻¹ and bond distances in angstroms.

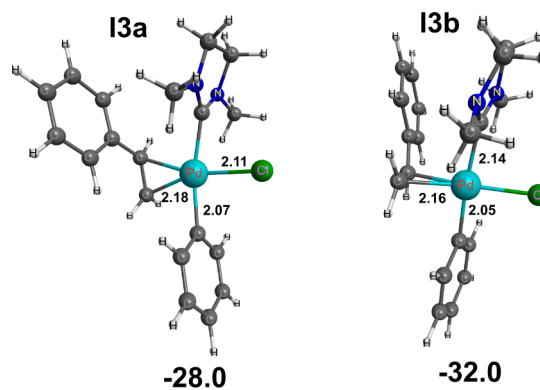


Figure 5. Starting intermediates, **13a** and **13b**, in the migratory insertion step. Relative energies are given in kcal mol⁻¹ and bond distances in angstroms.

orientation to the metal plane, whereas an olefin in-plane arrangement is observed in the case of the **13a** intermediate. **13b** is 4 kcal mol⁻¹ lower in energy than **13a**. Styrene rotation around the metal–olefin bond axis leads from **13b** to **13a**. The transition state going from **13a** to **13b**, **TS_13ab**, is -25.8 kcal mol⁻¹ with respect to the separated reactants and 6.8 kcal mol⁻¹ above **13b** (see the Supporting Information for more details about the **TS_13ab** geometry, as well the optimized geometries for all structures discussed in the text).

The migratory insertion of **9** into the Pd–C bond is usually the step responsible for the regioselectivity of the Heck reaction.^{28–30} This step has two associated transition states, **TS2a** and **TS2b** (Figure 6). The transition state **TS2a** involves the β -carbon styrene addition to the terminal carbon of the olefin double bond, while **TS2b** is responsible for the C–C bond formation between the α -carbon from the olefin and the aryl group (Figure 7). **TS2a** is connected to **13a**, and it is found 20.7 kcal mol⁻¹ below the separated reactants and 4.6 kcal

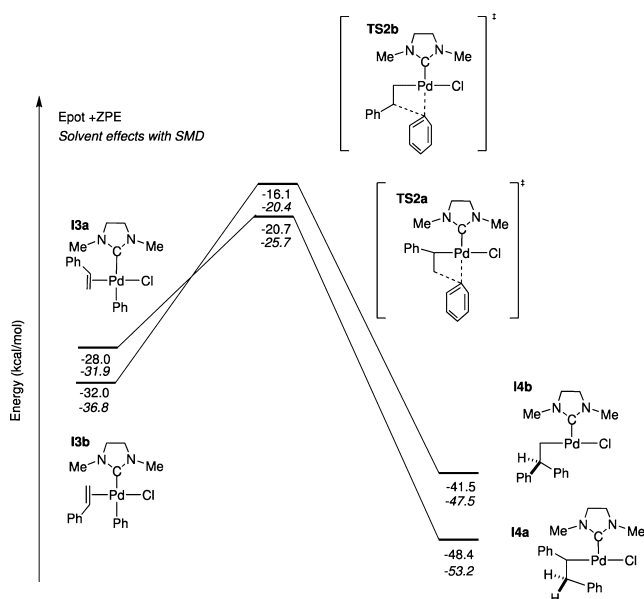


Figure 6. Migratory insertion step and the transition states, TS2a and TS2b, associated with the pathways. Relative energies are given in kcal mol⁻¹ with respect to the separated reactants.

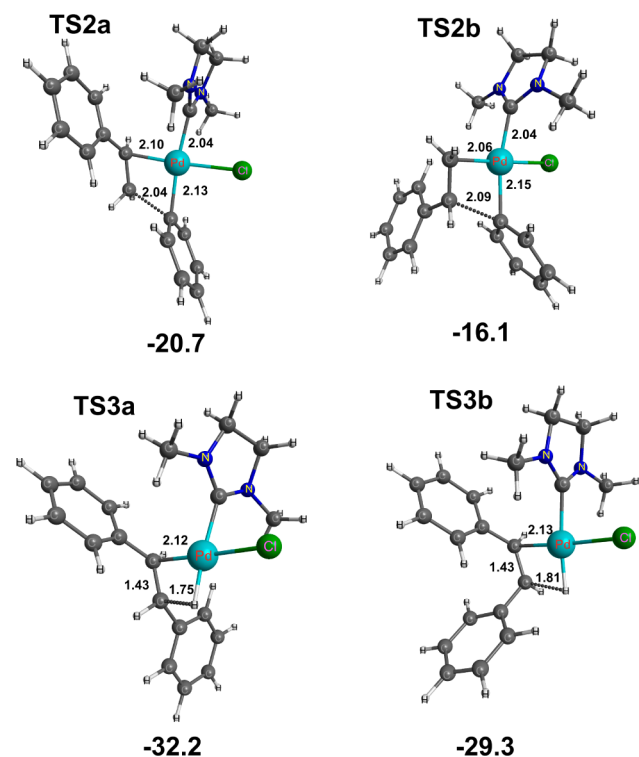


Figure 7. Analyzed TSs for the migratory insertion (TS2a and TS2b) and β -hydride *syn*-elimination (TS3a and TS3b) steps. Relative energies are given in kcal mol⁻¹ and bond distances in angstroms.

mol⁻¹ lower in energy than TS2b. The intermediate I4a is 6.9 kcal mol⁻¹ lower in energy than I4b, and it is expected to be the major product for the insertion process. This model reaction predicts a high regioselectivity of the (NHC)Pd-catalyzed C–C bond formation.

The following neutral process is the β -hydride *syn*-elimination. Previous reports have shown that the stereoselectivity is controlled in this step.^{31,32} Once more, there are

two competitive paths going through the transition states, TS3a and TS3b. Figure 7 shows their respective M06L/6-31+G(d)-optimized structures. To achieve such four-membered-ring transition states, it is necessary to reorient the β -hydrogen in the PhCH₂ group of I4a and I4b toward the metal center. After the isomerization of the intermediates I4a and I4b to the agostic intermediates I5a and I5b, the reaction takes place via the transition states TS3a and TS3b, respectively. Figure 8 displays the competitive pathways related to the β -

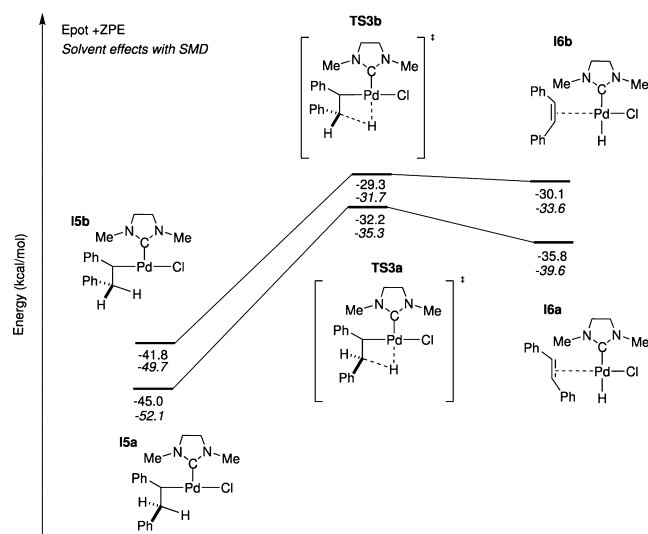
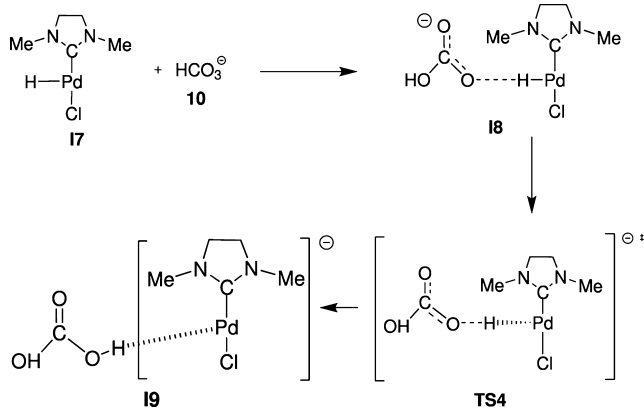


Figure 8. β -Hydride *syn*-elimination step and the pathways related to the transition states, TS3a and TS3b. Relative energies are given in kcal mol⁻¹ with respect to the separated reactants.

hydride *syn*-elimination. The energetics of the mechanism shows that this step is more likely to proceed via the transition state TS3a, which is 32.2 kcal mol⁻¹ below the separated reactants and about 3 kcal mol⁻¹ lower in energy than TS3b. Therefore, the *trans* Heck adduct (11) is expected as the major product. The intermediates I6a and I6b are respectively –35.8 and –30.1 kcal mol⁻¹ with respect to the reactants. However, such intermediates present higher relative energies than their related I5a and I5b, reflecting an endoergic process. When I6 intermediates are achieved, the product is already formed but remains coordinated to the metal center. The separation of 11 from Pd has an energy cost of 12.7 kcal mol⁻¹. After the Heck adduct 11 releases the metal center, the Pd-hydride complex I7 is formed. This intermediate is 23.1 kcal mol⁻¹ below the reactants.

The final part of the catalytic cycle is the reductive elimination step, which is depicted in Scheme 5. At this point, the metal center undergoes a reduction, Pd²⁺ → Pd⁰, and the starting active species [(NHC)PdCl]⁻ is regenerated. The HCO₃⁻ base is proposed as responsible for abstracting the proton from the palladium center. The reductive elimination occurs almost barrierlessly. The relative energy of the transition state associated with this step, TS4, is –48.0 kcal mol⁻¹, with respect to the separated reactants. This transition state develops a charge (the negatively charged active catalyst is being regenerated) and the impact of the solvent effect becomes more pronounced than during the neutral steps. It is worth mentioning, once again, that it does not change the overall trend over the energetic profile of the reaction. When solvent effects are included, the relative electronic energy is –35.8 kcal

Scheme 5. Reductive Elimination and Catalyst Regeneration



mol^{-1} with respect to the separated reactants. Figure 9 displays optimized geometries for 18 and TS4. 18 and TS4 have very

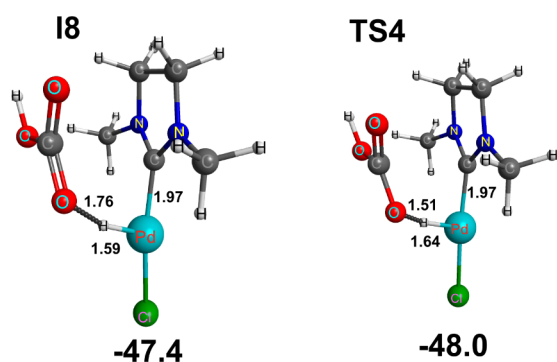


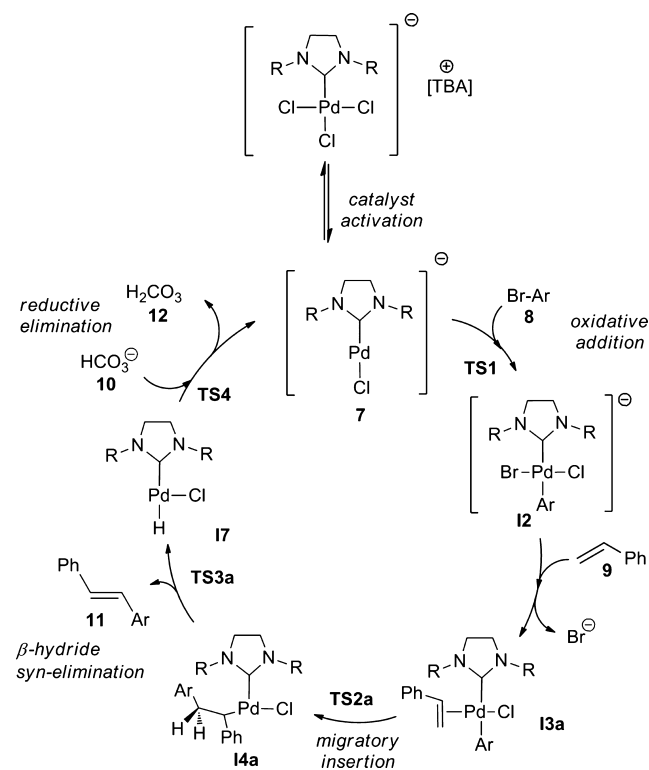
Figure 9. Optimized 18 and TS4 geometries for selected structures associated with the reductive elimination step. Relative energies are given in kcal mol^{-1} and distances in angstroms.

similar structures, with the main difference being the Pd–H bond distance, 1.59 and 1.64 Å, respectively. The protonated base, H_2CO_3 , is still bonded to the Pd in 19, which is 50.3 kcal mol^{-1} below the reactants. Finally, catalyst 7 is regenerated after the departure of H_2CO_3 (12).

In summary, a plausible Amatore–Jutand-type mechanism for a model Mizoroki–Heck reaction was explored by DFT calculations, based on our experimental results and the synthesis of a new [TBA][NHC]PdCl₃ complex. The potential energy profile presented revealed that a mechanistic proposal involving anionic (NHC)-palladium(0) species is feasible, through a combination of neutral and anionic steps and with high regio- and stereoselectivity (Scheme 6). Ongoing work aims to investigate other feasible pathways, including a more realistic model of the NHC ligand, as well as the application of this type of precatalyst to other Pd-catalyzed cross-coupling reactions.

EXPERIMENTAL SECTION

Synthesis of [TBA][SIPr]PdCl₃ (2). A reaction vial was loaded with a magnetic stirring bar, (SIPr)PdCl₂(TEA) (502 mg, 0.75 mmol), tetrabutylammonium chloride (231 g, 0.83 mmol), and 2 mL of dry acetone. The solution was allowed to stir at room temperature overnight. Removal of the solvent in vacuo afforded a yellow oil, which was dissolved in ethyl acetate and triturated with hexane to yield the title compound as a pale yellow solid (613 mg, 97%). ¹H NMR (500 MHz, C₆D₆); δ 7.28–7.20 (m, 6H), 3.88–3.79 (m, 4H), 3.55 (s, 4H), 3.16–3.09 (m, 8H), 1.77 (d, $J = 6.5$ Hz, 12H), 1.46–1.37 (m, 8H),

Scheme 6. Plausible Mechanism Pathway for the [(NHC)PdCl][−]-Catalyzed Mizoroki–Heck Reaction

1.33–1.25 (m, 8H), 1.20 (d, $J = 6.5$ Hz, 12H), 0.95 (t, $J = 7.3$ Hz, 12H). ¹³C{¹H} NMR (100 MHz, C₆D₆): δ 190.4, 147.6, 136.5, 128.5, 124.1, 58.3, 53.3, 28.6, 26.6, 24.7, 24.0, 19.7, 13.9. Anal. Calcd for C₄₃H₇₄Cl₃N₃Pd: C, 61.06; H, 8.82; N, 4.97. Found: C, 60.94; H, 8.77; N, 4.94.

General Procedure for Heck Reactions. In open air, a 4 mL screw-capped vial equipped with a magnetic stirring bar was charged with potassium carbonate (1 mmol), aryl halide (0.5 mmol), 2 (0.5 mol %), anhydrous DMF (1 mL), and the alkene (0.55 mmol). The vial was sealed with a screw-cap fitted with a septum, and the reaction mixture allowed to stir at 140 °C and monitored by gas chromatography. When the reaction was complete or there was no further increase in conversion, it was cooled to room temperature, poured into water (10 mL), and extracted with Et₂O or EtOAc (3 × 10 mL). The combined organic layers were washed with water (3 × 10 mL) and brine (10 mL), dried over MgSO₄, and filtered. The resulting solution was concentrated onto Celite under reduced pressure for purification by column chromatography. All reported yields are an average of two runs.

Computational Studies. All electronic structure calculations were carried out within the Kohn–Sham density functional theory (DFT) formalism^{33–35} with the Gaussian09 suite of quantum chemical programs.³⁶ The M06L³⁷ functional was used in the current study, because it has been proved to be an efficient and reliable method for transition metal thermochemistry.³⁸ The SDD basis set was adopted to Pd³⁹ and Br⁴⁰ atoms and the 6-31+G(d) basis set for the remaining atoms.⁴¹ Full geometry optimizations without any symmetry restriction followed by frequency calculations on all stationary points were performed to verify their nature as a minimum or a transition state (TS) on the potential energy surface. The vibrational analysis was performed within the harmonic approximation with thermochemical data calculated at 298 K and 1 atm. Intrinsic reaction coordinate (IRC)⁴² calculations were used to further authenticate doubtful TSs. Solvent effects were taken into account with the continuum solvation model SMD⁴³ with DMF as the solvent. The SMD calculations were performed as single-point energy calculations (SMD-M06L) on the M06L/6-31+G(d), SDD(Pd,Br) optimized gas-phase geometries. The

results obtained with this approach are denoted SMD-M06L/6-31+G(d)//M06L/6-31+G(d). The relative energies of all minima and TSs are presented in terms of potential energies including zero-point energy (ZPE) corrections. The results are not discussed in terms of free energies in solution, since the use of continuum solvation models combined with gas-phase rigid rotor-harmonic oscillator statistical mechanics can introduce significant errors to the discussion.⁴⁴ All energies are presented in kcal mol⁻¹ with respect to the infinitely separated reactants, unless otherwise specified.

■ ASSOCIATED CONTENT

● Supporting Information

Characterization of products and details on computational studies. This material is available free of charge via the Internet at <http://pubs.acs.org>.

■ AUTHOR INFORMATION

Corresponding Authors

*E-mail: ataualpa@iq.usp.br.

*E-mail: o.navarro@sussex.ac.uk.

Notes

The authors declare no competing financial interest. The findings in this paper are addressed in patent application GB1321706.2.

■ ACKNOWLEDGMENTS

O.N. gratefully acknowledges the Enterprise Development Fund of the University of Sussex for support. V.H.M.S. and A.P.L.B. are thankful to Fundação de Amparo à Pesquisa do Estado de São Paulo (grants 13/04813-6 and 13/22235-0).

■ DEDICATION

Dedicated to the memory of Prof. Mike Lappert.

■ REFERENCES

- (1) (a) Heck, R. F.; Nolley, J. P. *J. Org. Chem.* **1972**, *37*, 2320–2322. (b) Mizoroki, T.; Mori, K.; Ozaki, A. *Bull. Chem. Soc. Jpn.* **1971**, *44*, 581.
- (2) (a) Oestreich, M., Ed. *The Mizoroki-Heck Reaction*; John Wiley & Sons: Chichester, U.K., 2009. (b) de Meijere, A.; Diederich, F., Eds.; *Metal-Catalyzed Cross-Coupling Reactions*, 2nd ed.; Wiley-VCH: Weinheim, Germany, 2004. (c) Phan, N. T. S.; Van Der Sluys, M.; Jones, C. W. *Adv. Synth. Catal.* **2006**, *348*, 609–679. (d) Santos, C. I. M.; Barata, J. F. B.; Faustino, M. A.; Lodeiro, C.; Neves, M. G. P. M. S. *RSC Adv.* **2013**, *3*, 19219–19238. (e) Whitcombe, N. J.; Hii, K. K.; Gibson, S. E. *Tetrahedron* **2001**, *7449*–7476. (f) Kumar, A.; Rao, G. K.; Kumar, S.; Singh, A. K. *Organometallics* **2013**, *33*, 2921–2943. (g) Knowles, J. P.; Whiting, A. *Org. Biomol. Chem.* **2007**, *5*, 31–44.
- (3) Some representative examples: (a) de Vries, J. G. *Dalton Trans.* **2006**, 421–429. (b) Shaw, B. L.; Perera, S. D. *Chem. Commun.* **1998**, 1863–1864. (c) Ruan, J.; Iggo, J. A.; Berry, N. G.; Xiao, J. *J. Am. Chem. Soc.* **2010**, *132*, 16689–16699. (d) Montoya, V.; Pons, J.; Branchadell, V.; Garcia-Antón, J.; Solans, X.; Font-Bardía, M.; Ros, J. *Organometallics* **2008**, *27*, 1084–1091. (e) Fiddy, S. G.; Evans, J.; Nelsius, T.; Newton, M. A.; Tsoureas, N.; Tulloch, A. A. D.; Danopoulos, A. A. *Chem.—Eur. J.* **2007**, *13*, 3652–3659.
- (4) Amatore, C.; Carré, E.; Jutand, A.; M'Barki, M. A.; Meyer, G. *Organometallics* **1995**, *14*, 5605–5614.
- (5) This mechanism has also been suggested for soluble Pd(0) colloids or nanoparticles; see ref 3a.
- (6) (a) Amatore, C.; Jutand, A. *J. Organomet. Chem.* **1999**, *576*, 254–278. (b) Amatore, C.; Jutand, A. *Acc. Chem. Res.* **2000**, *33*, 314–321.
- (7) (a) Nolan, S. P., Ed. *N-Heterocyclic Carbenes: Effective Tools for Organometallic Synthesis*; Wiley-VCH: Weinheim, Germany, 2014. (b) Cazin, C. S. J., Ed. *N-Heterocyclic Carbenes in Transition Metal Catalysis and Organocatalysis*; Springer Science: Heidelberg, Germany,

2011. (c) Díez-González, S., Ed. *N-Heterocyclic Carbenes. From Laboratory Curiosities to Efficient Synthetic Tools*; RSC Publishing: London, U.K., 2010. (d) Glorius, F., Ed. *N-Heterocyclic Carbenes in Transition Metal Catalysis*; Springer Science: Heidelberg, Germany, 2007.

- (8) Gallop, C. W. D.; Zinser, C.; Guest, D.; Navarro, O. *Synlett* **2014**, 25, 2225–2228.
- (9) Jeffery, T. *J. Chem. Soc., Chem. Commun.* **1984**, 1287–1289.
- (10) Chen, M.-T.; Vicić, D. A.; Turner, M. L.; Navarro, O. *Organometallics* **2011**, *30*, 5052–5056.
- (11) (a) Goggin, P. L.; Goodfellow, R. R.; Reed, F. J. S. *J. Chem. Soc., Dalton Trans.* **1972**, 1298–1303. (b) Duddell, D. A.; Goggin, P. L.; Goodfellow, R. J.; Norton, M. G.; Smith, J. G. *J. Chem. Soc. A* **1970**, 545–564.
- (12) Huynh, H. V.; Han, Y.; Ho, J. H. H.; Tan, G. K. *Organometallics* **2006**, *25*, 3267–3274.
- (13) (a) Hermann, W. A.; Schwarz, J.; Gardiner, M. G. *Organometallics* **1999**, *18*, 4082–4089. (b) Heckenroth, M.; Kluser, E.; Neels, A.; Albrecht, M. *Dalton Trans.* **2008**, 6242–6249. (c) Zamora, M. T.; Ferguson, M. J.; McDonald, R.; Cowie, M. *Dalton Trans.* **2009**, 7269–7287. (d) Zamora, M. T.; Ferguson, M. J.; McDonald, R.; Cowie, M. *Organometallics* **2012**, *31*, 5463–5477.
- (14) Some recent examples in the literature: (a) Tessin, U. I.; Bantreil, X.; Songis, O.; Cazin, C. S. J. *Eur. J. Inorg. Chem.* **2013**, 2007–2010. (b) Gao, T.-T.; Jin, A.-P.; Shao, L.-X. *Beilstein J. Org. Chem.* **2012**, *8*, 1916–1919. (c) Lin, Y.-C.; Hsueh, H.-H.; Kanne, S.; Chang, L.-K.; Liu, F.-C.; Lin, I. J. B. *Organometallics* **2013**, *32*, 3859–3869. (d) Keske, E. C.; Zenkina, O. V.; Wang, R.; Crudden, C. M. *Organometallics* **2012**, *31*, 6215–6221.
- (15) Pytkowicz, J.; Roland, S.; Mangeney, P.; Meyer, G.; Jutand, A. *J. Organomet. Chem.* **2003**, *678*, 166–179.
- (16) Amarante, G. W.; Benassi, M.; Milagre, H.; Braga, A. A.; Maseras, F.; Eberlin, M. N.; Coelho, F. *Chem.—Eur. J.* **2009**, *15*, 12460–12469.
- (17) Pérez-Rodríguez, M.; Braga, A. A. C.; Garcia-Melchor, M.; Pérez-Temprano, M. H.; Casares, J. A.; Ujaque, G.; deLera, A. R.; Álvarez, R.; Maseras, F.; Espinet, P. *J. Am. Chem. Soc.* **2009**, *131*, 3650–3657.
- (18) García-Cuadrado, D.; Braga, A. A. C.; Maseras, F.; Echavarren, A. M. *J. Am. Chem. Soc.* **2006**, *128*, 1066–1067.
- (19) Braga, A. A. C.; Ujaque, G.; Maseras, F. *Organometallics* **2006**, *25*, 3647–3658.
- (20) García-Melchor, M.; Braga, A. A. C.; Lledós, A.; Ujaque, G.; Maseras, F. *Acc. Chem. Res.* **2013**, *46*, 2626–2634.
- (21) Carrow, B. P.; Hartwig, J. F. *J. Am. Chem. Soc.* **2010**, *132*, 79–81.
- (22) Phan, N.; VanDerSluys, M.; Jones, C. *Adv. Synth. Catal.* **2006**, *348*, 609–679.
- (23) Proutiere, F.; Schoenebeck, F. *Angew. Chem., Int. Ed.* **2011**, *50*, 8192–8195.
- (24) Goossen, L. J.; Koley, D.; Hermann, H. L.; Thiel, W. *J. Am. Chem. Soc.* **2005**, *127*, 11102–11114.
- (25) Goossen, L. J.; Koley, D.; Hermann, H. L.; Thiel, W. *Organometallics* **2006**, *25*, 54–67.
- (26) (a) Kozuch, S.; Shaik, S.; Jutand, A.; Amatore, C. *Chem.—Eur. J.* **2004**, *10*, 3072–3080. (b) Albert, K.; Gisdakis, P.; Rösch, N. *Organometallics* **1998**, *17*, 1608–1616.
- (27) Bode, B.; Gordon, M. S. *J. Mol. Graphics Mod.* **1998**, *16*, 133–138.
- (28) Bäcktorp, C.; Norrby, P.-O. *J. Mol. Catal. A: Chem.* **2010**, *328*, 108–113.
- (29) Dang, Y.; Qu, S.; Wang, Z.; Wang, X. *J. Am. Chem. Soc.* **2014**, *136*, 986–998.
- (30) Xu, L.; Hilton, M. J.; Zhang, X.; Norrby, P.-O.; Wu, Y.-D.; Sigman, M. S.; Wiest, O. *J. Am. Chem. Soc.* **2014**, *136*, 1960–1961.
- (31) Henriksen, S. T.; Tanner, D.; Cacchi, S.; Norrby, P.-O. *Organometallics* **2009**, *28*, 6201–6205.
- (32) Sköld, C.; Kleimark, J.; Trejos, A.; Odell, L. R.; Nilsson Lill, S. O.; Norrby, P.-O.; Larhed, M. *Chem.—Eur. J.* **2012**, *18*, 4714–4722.
- (33) Hohenberg, P.; Kohn, W. *Phys. Rev.* **1964**, *136*, B864–B871.

- (34) Kohn, W.; Sham, L. J. *Phys. Rev.* **1965**, *140*, A1133–A1138.
- (35) Parr, R. G.; Weitao, Y. *Density-Functional Theory of Atoms and Molecules*; Oxford University Press: New York, USA, 1994.
- (36) Frisch, M. J.; Trucks, G. W.; Schlegel, H. B.; Scuseria, G. E.; Robb, M. A.; Cheeseman, J. R.; Scalmani, G.; Barone, V.; Mennucci, B.; Petersson, G. A.; Nakatsuji, H.; Caricato, M.; Li, X.; Hratchian, H. P.; Izmaylov, A. F.; Bloino, J.; Zheng, G.; Sonnenberg, J. L.; Hada, M.; Ehara, M.; Toyota, K.; Fukuda, R.; Hasegawa, J.; Ishida, M.; Nakajima, T.; Honda, Y.; Kitao, O.; Nakai, H.; Vreven, T.; Montgomery, J. A., Jr.; Peralta, J. E.; Ogliaro, F.; Bearpark, M.; Heyd, J. J.; Brothers, E.; Kudin, K. N.; Staroverov, V. N.; Kobayashi, R.; Normand, J.; Raghavachari, K.; Rendell, A.; Burant, J. C.; Iyengar, S. S.; Tomasi, J.; Cossi, M.; Rega, N.; Millam, M. J.; Klene, M.; Knox, J. E.; Cross, J. B.; Bakken, V.; Adamo, C.; Jaramillo, J.; Gomperts, R.; Stratmann, R. E.; Yazyev, O.; Austin, A. J.; Cammi, R.; Pomelli, C.; Ochterski, J. W.; Martin, R. L.; Morokuma, K.; Zakrzewski, V. G.; Voth, G. A.; Salvador, P.; Dannenberg, J. J.; Dapprich, S.; Daniels, A. D.; Farkas, Ö.; Foresman, J. B.; Ortiz, J. V.; Cioslowski, J.; Fox, D. J. *Gaussian 09*, Revision D.01; Gaussian Inc.: Wallingford, CT, 2009.
- (37) Zhao, Y.; Truhlar, D. G. *Theor. Chem. Acc.* **2008**, *120*, 215–241.
- (38) Zhao, Y.; Truhlar, D. G. *Acc. Chem. Res.* **2008**, *41*, 157–167.
- (39) Andrae, D.; Huermann, U.; Dolg, M.; Stoll, H.; Preu, H. *Theor. Chim. Acta* **1990**, *77*, 123–141.
- (40) Bergner, A.; Dolg, M.; Kchle, W.; Stoll, H.; Preu, H. *Mol. Phys.* **1993**, *80*, 1431–1441.
- (41) Francl, M. M.; Pietro, W. J.; Hehre, W. J.; Binkley, J. S.; Gordon, M. S.; DeFrees, D. J.; Pople, J. A. *J. Chem. Phys.* **1982**, *77*, 3654–3665.
- (42) Hratchian, H. P.; Schlegel, H. B. *J. Chem. Theory Comput.* **2005**, *1*, 61–69.
- (43) Marenich, A. V.; Cramer, C. J.; Truhlar, D. G. *J. Phys. Chem. B* **2009**, *113*, 6378–6396.
- (44) Harvey, J. N. *Faraday Discuss.* **2010**, *145*, 487–505.